LUND UNIVERSITY

Design of an extreme-ultraviolet monochromator free from temporal stretching

Norin, Johan; Osvay, Karoly; Albert, F; Descamps, D; Yang, JJ; L'Huillier, Anne; Wahlström, Claes-Göran

Published in:
Applied Optics

2004

Link to publication

Citation for published version (APA):
Norin, J., Osvay, K., Albert, F., Descamps, D., Yang, JJ., L'Huillier, A., & Wahlström, C.-G. (2004). Design of an extreme-ultraviolet monochromator free from temporal stretching. *Applied Optics*, *43*(5), 1072-1081. http://www.opticsinfobase.org/abstract.cfm?URI=ao-43-5-1072

Total number of authors:
7

General rights
Unless other specific re-use rights are stated the following general rights apply:
Copyright and moral rights for the publications made accessible in the public portal are retained by the authors and/or other copyright owners and it is a condition of accessing publications that users recognise and abide by the legal requirements associated with these rights.
• Users may download and print one copy of any publication from the public portal for the purpose of private study or research.
• You may not further distribute the material or use it for any profit-making activity or commercial gain
• You may freely distribute the URL identifying the publication in the public portal

Read more about Creative commons licenses: https://creativecommons.org/licenses/

Take down policy
If you believe that this document breaches copyright please contact us providing details, and we will remove access to the work immediately and investigate your claim.

LUND UNIVERSITY

PO Box 117
221 00 Lund
+46 46-222 00 00

Download date: 17. Dec. 2025

Design of an extreme-ultraviolet monochromator free from temporal stretching

Johan Norin, Karoly Osvay, Francois Albert, Dominique Descamps, Jianjun Yang, Anne L'Huillier, and Claes-Göran Wahlström

High-order harmonic generation in gases by use of femtosecond lasers is a source of ultrashort pulses in the extreme-ultraviolet (XUV). For many applications it is necessary to select radiation of only one specific harmonic order without affecting the duration of the ultrashort pulse. A three-grating monochromator that meets this demand has been designed and modeled by ray tracing as well as by wave-optical simulations. The only remaining temporal stretching of an XUV pulse is due to distortion of the pulse front on the gratings and is predicted to be ~1 fs. The design has been successfully tested in the near infrared. Finally, the monochromator is also capable of eliminating any existing linear chirp in the harmonic pulses, thus compressing them to shorter durations. © 2004 Optical Society of America

OCIS codes: 190.4160, 120.4140, 320.5520, 050.1590.

1. Introduction

Interest in using high-order-harmonic generation in gases as a coherent source of extreme-ultraviolet (XUV) radiation has grown rapidly during the past 10 years. Although other XUV sources are available (synchrotron radiation is the most common), high-order harmonic generation is the obvious option if extremely short pulses or high peak power is required. High harmonics are created when an intense laser pulse is focused into a gas[1,2] and have been used in, e.g., pump–probe lifetime measurements,[3,4] time-resolved surface physics,[5] molecular physics,[6] two-photon ionization,[7,8] and XUV interferometry.[9]

For high-harmonic generation the laser's intensity has to be near 10^{14} W/cm^2, which one can easily achieve by focusing pulses from modern short-pulse laser systems. The fundamental pulse can be focused into a gas jet, a gas cell, or a gas-filled hollow fiber,[10,11] and several gases can be used.[12] The generation is a highly nonlinear process, and the radiation properties depend on several parameters: pulse duration, laser energy and wavelength, spatial beam mode and diameter, and focusing conditions.[13] The harmonics, of odd order for symmetry reasons, have similar intensities up to a cutoff energy that depends on the laser's intensity and the nonlinear medium. Harmonics with photon energies as high as ~500 eV have been produced by use of intense ultrashort driving pulses.[14,15] The different harmonics are emitted simultaneously from the medium and propagate together with the fundamental laser pulse.

In many applications it is important to be able to select one of these harmonics without affecting its temporal characteristics as well as to suppress the several-orders-of-magnitude stronger laser pulse used in the harmonic generation. The short-wavelength transmission of various metals and their different absorption edges of these metals make them useful as wavelength filters. Free-standing metal films can be made thin to minimize absorption and distortion of the transmitted part of the pulse.[6] However, inasmuch as transmission and absorption occur in broad energy bands, these filters are more suitable as high- or low-pass filters than for extraction of single harmonics.

Dielectric multilayer mirrors can be optimized for narrow-wavelength intervals in the XUV region, but the reflectivity decreases for shorter wavelengths. Also, it is difficult to manufacture a mirror that reflects only in a narrow XUV wavelength band. Even though the reflectivity of the fundamental beam can be made low, the reflected part can still be significant

The authors are with the Department of Physics, Lund Institute of Technology, P.O. Box 118, SE-221 00 Lund, Sweden. K. Osvay is on leave from the Department of Optics, University of Szeged, Szeged, Hungary. A. L'Huillier's e-mail address is anne.lhuillier@fysik.lth.se.

Received 5 June 2003; revised manuscript received 30 September 2003; accepted 15 October 2003.
0003-6935/04/051072-10$15.00/0
© 2004 Optical Society of America

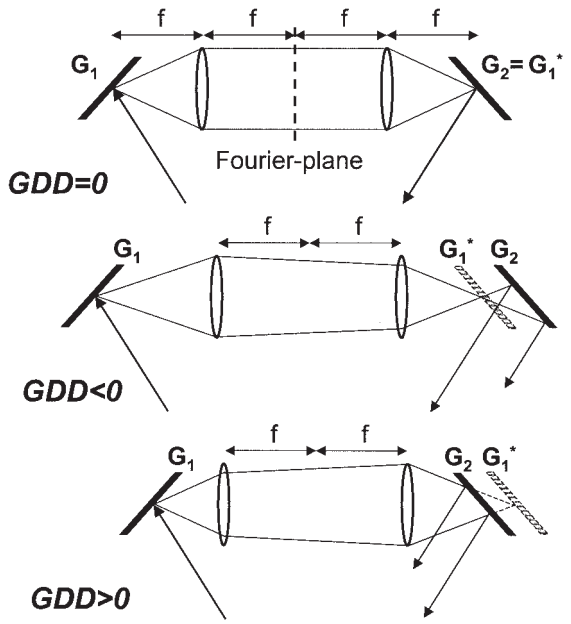

Fig. 1. Schematic of a grating-pair stretcher consisting of two plane gratings (G_1 and G_2) and two lenses. If grating G_1 is imaged onto G_2, then the resultant GDD is zero and pulse shaping including the selection of a spectral range takes place in the common Fourier plane of the lenses. If the image of G_1 lies before or behind G_2, then the resultant GDD is negative (b) or positive (c), respectively. For more details see Subsection 1.A.

because the radiation at the fundamental frequency is typically 6–9 orders of magnitude higher than the harmonics. If a spectrally clean beam is wanted, a combination of metal filters and mirrors can be used, but a battery of them will be needed to make tunability possible over a large spectral region.

Selection of a spectral range without causing temporal stretching has been made in the visible and the infrared[17–19] in a zero group-delay dispersion device (Fig. 1). Adaptation of this idea to the vacuum ultraviolet and the XUV, however, is not straightforward because of the lack of transmission optics in this spectral region. An all-reflective optics variation with plane gratings, which is used mostly as a stretcher in chirped-pulse amplification laser systems,[17,20,21] always leads to phase shifts that are proportional to the distance between the gratings. Recently a Michelson interferometer design that is based on the zero-dispersion principle and uses reflective optics and a single free-standing transmission grating, double passed in the first order, was proposed by Goulielmakis *et al.* as a diagnostic tool for ultrashort harmonic radiation.[22] Although this setup could also work as a short-pulse monochromator, it gives no freedom to compensate for any existing chirp in the pulse.

In the present paper we propose a grating configuration derived from one suggested by Villoresi,[23] which uses two spherical gratings set in an asymmetric configuration. A setup based on this idea, which uses one spherical and one toroidal grating, was recently experimentally developed and even applied.[6,24] In our setup we add a free-standing transmission grating at near-normal incidence in the focal plane of the first grating. This allows us to suppress the residual temporal chirp of the curved grating pair, together with any other linear chirp in the radiation, resulting in a compressed pulse with higher peak power. In Section 1 we outline the basic ideas behind our design. In Section 2, numerical results from ray tracing as well as wave propagation calculations are presented. Because of the inherent difficulties in measuring the durations of femtosecond XUV pulses, we have chosen first to build a prototype and to make a proof-of-principle experiment in the near-infrared region (800 nm) for which sensitive measurement techniques are well developed. The results of these measurements are discussed in Section 3. Comparing the results from the experiment with theoretical results obtained for 800 nm allows us to verify the validity of our theoretical approach and thereby also the predictions for XUV harmonic pulses, which are discussed in Section 4.

1. Theoretical Background

A. General Considerations

Almost all highly efficient and widely tunable wavelength selectors, e.g., monochromators and spectrometers, rely on angular dispersion of one or more optical elements. However, optical elements (such as gratings and prisms) that have angular dispersion always change—usually lengthen—an ultrashort pulse in time, because of two effects: chirping and pulse-front tilting. As will be shown, the first effect is more pronounced for broader-bandwidth pulses, whereas the second effect becomes significant for short pulses propagating in large-diameter beams.

The general description of the chirping effect is based on the calculation of the spectrally dependent optical path $P(\omega)$ from the disperser to the point of observation.[25] Assuming that there is no other dispersive material in the system, the optical path depends on the angular dispersion of the system simply as

$$P(\omega) = L \cos \theta, \qquad \theta = \theta(\omega), \tag{1}$$

where L is the distance between the source of angular dispersion and the position of observation along the ray of the central frequency, ω_0, and θ is the angle between the rays of ω_0 and an arbitrary frequency, ω (Fig. 2). If the angular disperser can be described by Fermat's law (see Subsection 2.A below), the phase $\phi(\omega)$ of a plane-wave ultrashort pulse will change on propagation as

$$\phi(\omega) = \frac{\omega}{c} P(\omega) = \frac{\omega}{c} L \cos \theta(\omega). \tag{2}$$

The first and second derivatives of ϕ with respect to ω are the group delay (GD) and the group-delay dispersion (GDD), respectively. If the GD is different for each spectral component, i.e., GDD $\neq 0$, then the pulse is temporally chirped and hence length-

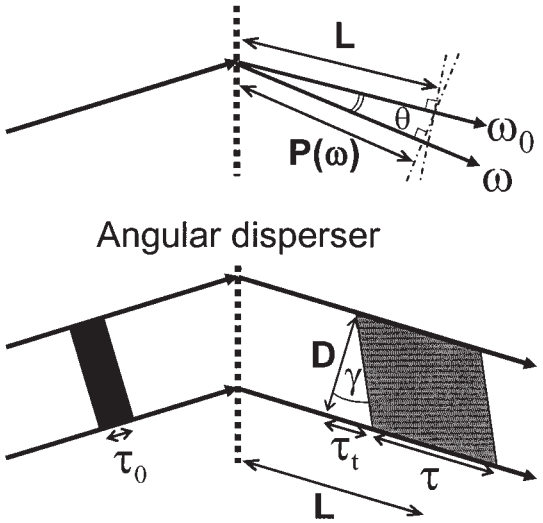

Fig. 2. Effect of angular dispersion on the duration of a laser pulse. The pulse becomes chirped and tilted, and the pulse duration is temporally lengthened from τ_0 to $\tau + \tau_t$. For more explanations, see text.

ened (Fig. 2). Assuming transform-limited Gaussian input pulses, the length of the output pulse is

$$\tau = \tau_0 \left[1 + \left(4 \ln (2) \frac{\mathrm{GDD}}{\tau_0^{\,2}} \right)^2 \right]^{1/2}, \tag{3}$$

where τ_0 is the transform-limited FWHM pulse length.[19] Similar, but somewhat more complicated, expressions are valid for non-transform-limited pulses[26,27] as well as for sech^2 pulses.[28]

It is worth noting that, following from Eqs. (1) and (2), the GD depends on the angular dispersion ($\mathrm{d}\theta/\mathrm{d}\omega$), whereas the GDD is a function of both $\mathrm{d}\theta/\mathrm{d}\omega$ and $\mathrm{d}^2\theta/\mathrm{d}\omega^2$. In addition, the chirp ($\mathrm{d}\omega/\mathrm{d}t$) that is due to single-element angular dispersion can be shown always to be negative; hence the GDD is also negative. This means that the short-wavelength (blue) components of the ultrashort pulse leave the angular disperser first, whereas the long (red) components are the last,[25] just the opposite of what would occur for a normally dispersive material.

Another important effect of angular dispersion is the tilt of the pulse front, which is due to the finite beam size of the incident pulse.[25,29] An exact wave-optical description of the problem was given by Martinez[30,31] and rediscovered recently by Pretzler *et al.*[32] Whereas in these approaches certain optical elements have been assumed, a device-independent theory[33] proved the general relation

$$\tan \gamma = \omega \frac{\mathrm{d}\theta}{\mathrm{d}\omega} \tag{4}$$

between the angle of tilt (γ) and angular dispersion.

The tilted pulse front leads to an even longer pulse duration in the plane of observation or in the plane of focus.[32,34] The stretch that is due only to pulse-front tilt can be calculated as

$$\tau_t = \frac{D}{c} \tan \gamma = \frac{D}{c} \omega \frac{\mathrm{d}\theta}{\mathrm{d}\omega}, \tag{5}$$

where D is the beam diameter after the element (Fig. 2). This picture is exact when the beam diameter D is much larger than the lateral spectral displacement of the beam that is due to angular dispersion, i.e.,

$$D \gg \Delta\omega \frac{\mathrm{d}\theta}{\mathrm{d}\omega} L.$$

The larger the beam diameter, the larger the temporal stretch τ_t. This effect, fortunately, can be completely canceled by use of a second angularly dispersive element that has the opposite sign of angular dispersion.

Unlike the pulse-front tilt [Eq. (5)], the temporal stretch that is due to GDD depends on the square of the angular dispersion [Eq. (3)], so a short pulse leaving such a double-element system is still chirped and hence is temporally lengthened. This is the basic principle behind existing pulse stretchers and compressors used in chirped-pulse amplification systems.

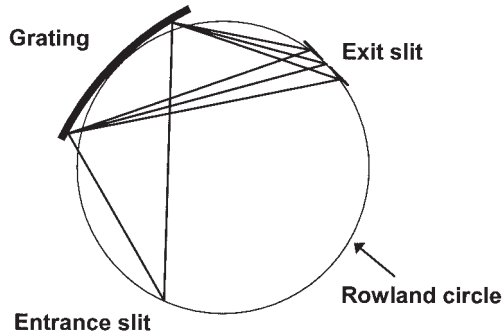

Fig. 3. Schematic of a spherical grating in the Rowland configuration.

B. Use of Spherical Gratings

The use of optics with finite focal length can, however, make the picture more complicated. As illustrated in Fig. 1, the GDD of a grating pair can be negative, zero, or positive, depending on the imaging conditions within the device.[17,18] In the XUV, where no lenses are available, an element that provides a good combination of focusing and angular dispersion is the spherical grating.

A single spherical grating used in the Rowland configuration[35] places each frequency component of an ultrashort pulse, diverging from the entrance slit, on the perimeter of the Rowland circle (Fig. 3). The propagation time to the perimeter of the circle is different for each of the constituent frequencies of the short pulse; hence the pulse becomes chirped. Because the grating is curved, the pulse front is not only tilted with respect to the phase front of the center frequency, as in the case of a plane grating, but is also curved.

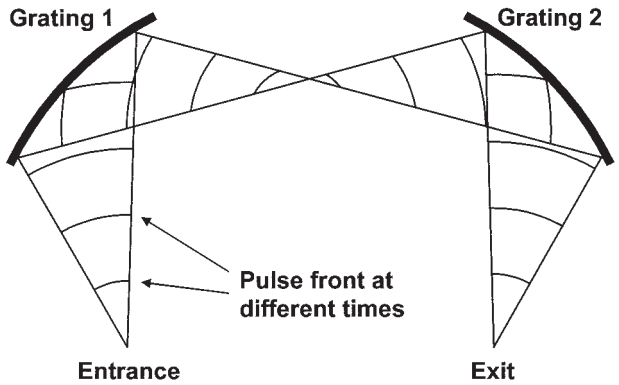

Fig. 4. Two-grating setup. The second grating is made to compensate for the pulse-front tilt introduced by the first grating. The pulse, however, becomes strongly chirped.

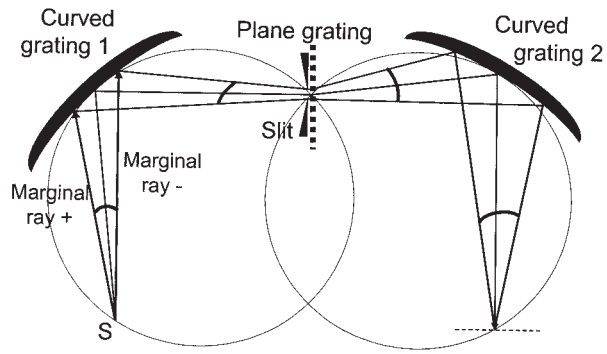

Fig. 5. Three-grating setup. The added transmission grating cancels the chirp introduced by the two spherical gratings but slightly tilts the wave front. The slit selects a central wavelength and a wavelength range.

Compensation for such a curved and tilted pulse-front is not an easy task. It requires a device that is capable of providing each frequency component with an opposite GD as it arrives at the perimeter. The best solution would be for each spectral component to be retroreflected. Unlike for plane gratings,[18] such a device cannot be simply constructed. The other solution is that the exit plane of one Rowland grating be imaged by a second Rowland grating under identical conditions (Fig. 4), with identical incident and emerging angles for the spectral components.[23] In this case the pulse-front tilt, similarly to that of the plane gratings, can be fully compensated for. The optical imaging properties of this curved grating pair are similar to those of a positive GDD pulse stretcher [Fig. 1(c)]. Thus pulses leaving this system are always positively chirped. In addition, the pulse-front curvature is not compensated for by the second grating; it even increases. A pulse leaving the two-spherical-grating system therefore presents a temporal stretch owing to the uncompensated positive chirp of the system and a spatial pulse-front distortion that is due to the mismatch between the two Rowland circles and the pulse-front curvature. It is quite obvious that the larger the diameter of the Rowland circles or the smaller the required bandwidth, the better the compensation. These conclusions, however, set a limit on the shortest XUV pulse obtainable with this scheme, which can be in the range of tens of picoseconds.

It is worth noting that the origin of the residual pulse-front curvature can also be explained by use of a different argument. As was pointed out in the aberration theory of the curved diffraction grating stretcher,[36] such a system always has a chromatic focusing error because different spectral components reach different parts of the off-axis spherical focusing element. (The focal length for each spectral component is different because of spherical aberration and astigmatism.) Chromatic focusing—or chromatic imaging—always leads to pulse-front distortion,[37–39] which broadens the pulse temporally. The chromatic focusing error of a two-curved-grating setup can hence be small if gratings with large radii of curvature are used and if the harmonic bandwidth is not too large.

C. Intermediate Transmission Grating

To compensate for the large positive chirp of the spherical grating pair, let us insert a transmission grating between the two spherical gratings (Fig. 5). The most obvious effect of this additional grating is that, as a single angular disperser (Subsection 1.A), it provides the pulse with a negative chirp. In addition, the characteristics of the new grating can be chosen such that this extra chirp also compensates for any linear chirp that was originally present in the pulse. This intermediate grating will also cause a pulse-front tilt, however, which may remain uncompensated for throughout the system. By using a small-diameter beam at the grating, one can make the pulse lengthening that is due to this pulse-front tilt smaller by at least 1 order of magnitude than the stretch caused by the uncompensated chirp of the grating pair (Fig. 2 and Eqs. (3) and (5)].

A schematic representation of our XUV monochromator is shown in Fig. 5. It consists of two curved gratings and an intermediate plane grating placed approximately on the Rowland circles of both gratings where the radiation is focused (therefore minimizing the induced pulse-front tilt). The desired wavelength range can be selected by an appropriately wide slit at the intermediate grating, whereas the center wavelength is determined by the position of the slit. The pulses leaving such a system are practically unchirped but exhibit some residual pulse-front tilt.

Because an analytical description of such a complicated system is not straightforward, we performed numerical simulations for the two designs (with and without the chirp-compensating transmission grating), using a ray-tracing program and through more-realistic electromagnetic-field propagation calculations.

2. Numerical Methods

A. Ray-Tracing Calculations

For optical elements that obey the leading principle of geometrical optics, Fermat's principle, it is straightforward to use the ray-tracing method for computing the phase shift of an ultrashort pulse, which one usually does by calculating the spectrally dependent optical path. The direct adaptation of this technique for diffraction gratings is physically incorrect because a grating selects the direction of diffraction by interference, which cannot be handled by geometrical optics. Treacy[40] intuitively assumed that the diffraction process on a pair of gratings introduces an extra phase shift φ_d, which leads to the total phase

$$\phi_g(\omega) = (\omega/c)P_g(\omega) + \varphi_d(\omega). \tag{6}$$

Here P_g is the spectrally dependent optical path between the gratings and φ_d depends on the number of grooves illuminated in the second grating.

Brorson and Haus[41] elegantly showed that diffraction gratings satisfy Fermat's principle provided that Eq. (6) is used to account for diffraction. In this way Treacy's main result was also proved[25,40]; that is, P_g gives the GD directly through the system as

$$\mathrm{GD}(\omega) = \frac{\mathrm{d}\phi_g}{\mathrm{d}\omega} = \frac{P_g(\omega)}{c}, \tag{7}$$

because the derivatives of $\varphi_d(\omega)$ and $P_g(\omega)/c$ cancel each other. Hence, calculating the optical path through the system from the source to the exit reference plane provides us directly with the GD.

For small beam diameters and for optical systems that satisfy the criteria of paraxial optics, i.e., when aberrations are negligible, the optical paths for the chief (central) ray and the marginal (peripheral) rays are the same. For larger beams and nonparaxial optics, however, the different types of aberration also result in pulse-front distortion, which may have a strong effect on the pulse duration at the target.[38,39,42] To account for spherical aberration and astigmatism we developed a ray-tracing program that calculates the optical path length along the chief ray as well as the marginal rays from the source (S) to the plane perpendicular to the chief ray of the central frequency at the focal point of the last grating (Fig. 5). This is done for all the frequency components of the pulse as well as for the ray components of the input beam, thus simulating the divergence and bandwidth of a real pulse. The spectrally and spatially dependent GD, that is, the pulse front, is then calculated. In the case of three gratings the program also minimizes the temporal stretch, either by varying the line density of the transmission grating or by rotating the grating while keeping the line density fixed.

The temporal stretch of a pulse is calculated as the GD difference between the spectral components at the half-maxima of the bandwidth. This estimation is correct only for large stretches, such that GDD $\gg$ τ_0^2. For small GDD it overestimates the stretched pulse length [Eq. (3)].

To test our new scheme we carried out the calculations first for the near-infrared region, where direct experimental verification could easily be achieved (see Section 3 below). Please note that the measure of any type of pulse broadening is several orders of magnitude less for pulses in the XUV region than in the near-infrared region (see Section 4 below). The operation of the optical setup in both regions, however, in principle is identical.

Figure 6 presents results obtained for the spectral range 780–820 nm for conditions close to the experimental ones. The groove density and the radius of curvature of the curved gratings were 580 lines/mm and 1 m, respectively. The divergence of the input beam was 2 mrad. Throughout the calculations, the marginal rays represent the FWHM divergence of the beam. Figure 7 is a simple sketch drawn to facilitate the understanding and interpretation of the results shown in Fig. 6. It illustrates the relationship of the variation of the GD as a function of wavelength for the marginal and chief rays to the pulse stretches that are due to the positive chirp (τ) and to the pulse-front tilt (τ_t).

For the two-grating setup [Fig. 6(a)], the GD depends strongly on the wavelength, suggesting a temporally chirped and stretched output pulse. The GD differences between the marginal rays at 780, 800, and 820 nm (not visible in the figure) are 124, 2, and 71 fs, respectively, which is a sign of the chromatic imaging error mentioned above and the subsequent pulse-front curvature. The measure of this pulse-front distortion is, however, much less than the chirp effect; the latter results in a temporal stretch as large as τ = 36.5 ps for a short pulse with a 20-nm bandwidth.

In the three-grating arrangement the intermediate grating was first chosen to have a groove density of 530 lines/mm and a 12° angle relative to the plane perpendicular to the chief ray, minimizing the pulse-front tilt at the central wavelength. The pulse-front distortion at 780, 800, and 820 nm leads to 86-, 5.5-, and 69-fs differences, respectively, between the marginal rays, which is a slight improvement on the two-grating case. The temporal stretch that is due to chirp is 2.9 ps, more than 1 order of magnitude less than in the two-grating case.

By optimizing the grating angle with respect to the overall GD difference we found that the 530-line/mm grating should be rotated to an angle −10.7° [dashed curves in Figs. 6(b) and 6(c)]. The residual small chirp results from the difference between the third- (and higher-) order dispersions of the plane grating and the curved gratings, and the pulse stretch that is due to chirp is reduced to only 280 fs, which is a more than 2-orders-of-magnitude improvement over the two-grating case. The pulse-front distortion, however, becomes more serious, because $\tau_t(780)$ = 785 fs, $\tau_t(800)$ = 741 fs, and $\tau_t(820)$ = 701 fs.

Further optimization led to groove densities of 560 lines/mm with a grating angle equal to 0° and 575

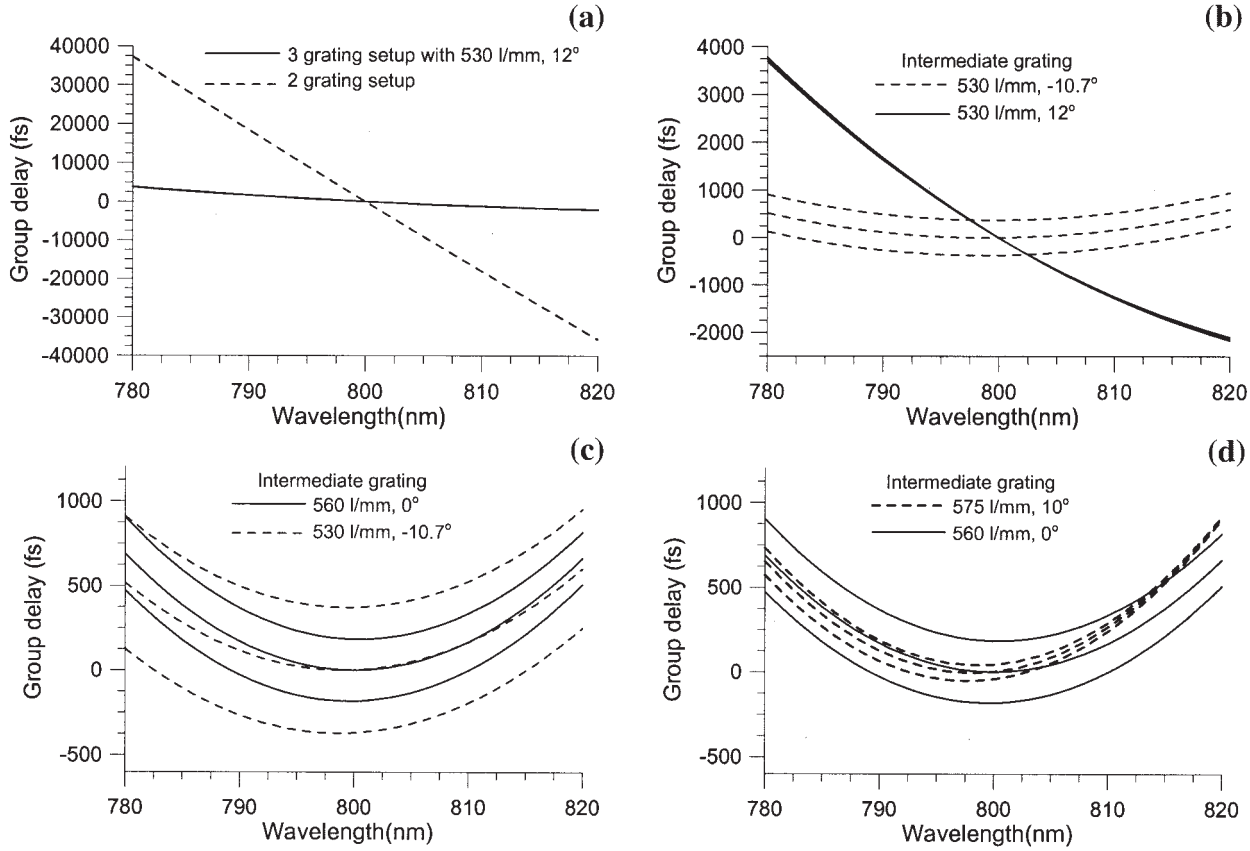

Fig. 6. Results of the ray-tracing calculations for several grating configurations. For explanations, see text.

lines/mm with a grating at 10°. As can be seen from Figs. 6(c) and 6(d), the chirp effect is practically the same as in the previous case, 332 and 390 fs, respectively. The pulse-front tilt is reduced to $\tau_t(780)$ = 428 fs, $\tau_t(800)$ = 366 fs, and $\tau_t(820)$ = 337 fs in the first case and $\tau_t(780)$ = 161 fs, $\tau_t(800)$ = 85 fs, and $\tau_t(820)$ = 15 fs in the second.

We therefore obtain overall pulse stretching below 500 fs, which means a more than 2-orders-of-magnitude improvement over the 36.5 ps offered by the two-grating arrangement. The optimal choice of the intermediate grating depends on the bandwidth and the divergence of the incoming pulse. For small bandwidth and large divergence, minimizing the pulse-front tilt gives the best result (530 lines/mm, 12°). If the pulse has a large bandwidth but a small divergence, minimizing the chirp effect leads to the shortest pulses.

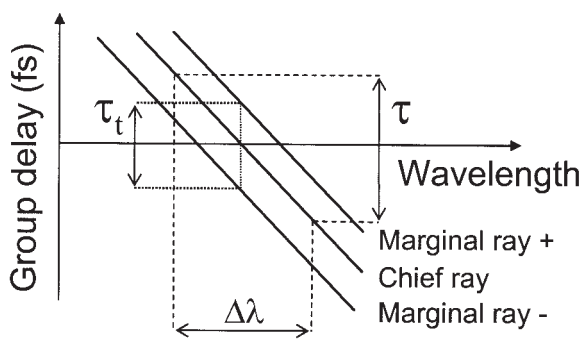

Fig. 7. Illustration of the contributions to the temporal stretch. The GD variation over the bandwidth of the pulse along the chief ray gives the temporal stretch that is due to chirp; the GD between the two marginal rays at a given wavelength represents the pulse-front distortion. See also Fig. 2.

B. Wave-Optical Approximation

The need to consider interference effects led us also to develop a more-realistic program based on the propagation of electromagnetic fields. We explain the method here for the two-grating setup. We start with a source point S at a given time (t = 0). The program first calculates the distance from the source point to all the grooves of the first grating. These become new source points according to Huygens's principle. Then the distances from these points to all the grooves of the next grating are calculated. Finally, the distance from each groove on the second grating to the target line (in the x direction) is calculated. This target line is placed at the position of the focus of the second grating. The path lengths are calculated for all combinations of paths from the original source point to the different target points. This information allows us to construct a two-dimensional target function $f(x, t)$ that describes how many paths end up at position x and at what time. Note that the number of paths to consider in this approach is much

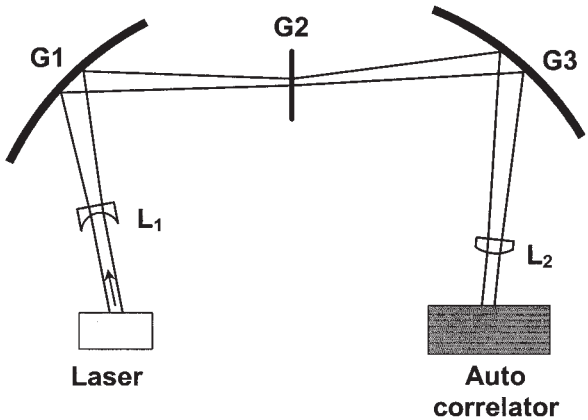

Fig. 8. Experimental setup. The negative lens L_1 creates a virtual focus at the entrance position of the first grating, G1. After the three gratings, the beam is collimated by the cylindrical lens, L_2. The pulse length is measured either by an autocorrelator or by a streak camera. To measure the pulse length before the gratings we inserted the autocorrelator before L_1.

larger than in the ray-tracing program, because the paths do not obey ray-optics laws. This calculation does not depend on wavelength. We account for the divergence by assigning a weight to each of the paths, depending on the incident angle on the first grating, thus simulating the intensity distribution of a Gaussian beam with a known diameter. The electrical field at position x and time t is given by the convolution of the electrical field at the source point and the response function of the optical system. For a Gaussian pulse, for example,

$$E(x, t) = \int f(x, t' - t)\exp(i\omega t') \times \exp[-2\ln(2)t'^2/\tau^2]\mathrm{d}t', \qquad (8)$$

where ω is the central frequency. The complexity of the calculation depends strongly on the number of diffractive planes, and the calculations become time consuming if more than two gratings are considered.

For the two-grating configuration we find that the two calculations presented above give almost identical results. This result gives us confidence in the validity of the ray-tracing predictions for the three-grating setup also.

3. Experimental Results

To test our proposed three-grating setup and to check the reliability of the simulations we performed a proof-of-principle experiment, using 17-nm-bandwidth, 50-fs pulses at 800 nm from a 10-Hz Ti:sapphire laser system. The experimental setup is shown in Fig. 8. The two spherical gratings have a radius of 1 m and a density of 580 lines/mm over a 40-mm square area. Both are mounted in a Rowland configuration with an incidence angle of 40° on the first grating. The gratings used in this experimental demonstration are not designed for high-power applications, and the pulses have to be heavily attenuated before the first grating to prevent optical damage. This is done with the combination of a half-wave plate and a polarizer. A negative lens is used to create a virtual source point at the entrance slit position of the first grating. There are two apertures, one before the first grating to allow us to simulate different divergences of the incoming beam and one near the exit slit position of the first grating (see Fig. 5) to control the bandwidth of the transmitted pulse. After the two gratings the beam is astigmatic and a cylindrical lens is used to collimate it.

To test the three-grating configuration we replaced the second aperture with a transmission grating with 530 lines/mm. The width of this grating was 20 mm, which was sufficient to avoid significantly cutting the spectrum. The grating was mounted and rotated to an incidence angle of 12°, determined by the optimization routine in the ray-tracing simulation described above. The second spherical grating was then slightly repositioned to the first order of the transmission grating.

The duration of the outcoming pulse was first determined by a streak camera (Hamamatsu C1587), which has sufficient resolution for the two-grating setup. The pulse length after the three-grating configuration, however, fell below the resolution of the streak camera and was instead measured with a single-shot second-order intensity autocorrelator placed in the exit position of the second spherical grating. This autocorrelator is not able to detect the temporal lengthening of a short pulse caused by pulse-front distortion, so only the broadening caused by the residual chirp could be measured. As our primarily aim was to compensate for the induced chirp in the two-grating setup, this type of autocorrelator was appropriate for our purpose.

It is worth noting that the procedure for aligning the two curved gratings is robust and straightforward.[23,36] On insertion of the plane grating, the output pulse's length immediately decreases, so one can quickly achieve the final alignment of the plane grating (position and tilt) by looking at the beam's spatial profile and the pulse width simultaneously.

The results of the experiments as well as of the numerical simulations are given in Table 1. For the two-grating setup, both types of simulation predict that the pulse will be stretched to above 30 ps, which

Table 1. Comparison of Simulated and Experimental Pulse Lengths after Passage of Near-Infrared Pulses through the Setup

Setup	Pulse Length (ps)	
	Ray-Tracing Simulated Results	Experimental Results
Two gratings, full spectrum[a]	31.2	32
Two gratings, 13-mm aperture between gratings	20.3	20
Three gratings	0.106	0.110

[a]This setup was also simulated with the wave propagation program, which gave a pulse length of 30 ps.

Table 2. Calculated Stretches of High Harmonics of an 800-nm Laser Pulse

Harmonic Order	Grating Density for Spherical Gratings (lines/mm)	Stretch[a] (fs)	
		Two-Grating Setup	Three-Grating Setup
9	200	150	0.16
9	400	570	0.71
9	600	1200	1.8
9	800	2,100	3.9
17	200	15	0.06
17	400	60	0.14
17	600	130	0.28
17	800	230	0.51
33	200	1.5	0.029
33	400	6.0	0.061
33	600	13	0.095
33	800	23	0.14
65	200	0.18	0.014
65	400	0.65	0.029
65	600	1.4	0.044
65	800	2.5	0.059

[a]These numbers represent the stretch of a delta pulse passing through the setup. The actual output pulses can be obtained by convolution with the input pulses.

was confirmed by the streak-camera measurements. This stretch is caused by the chirp introduced by the two curved gratings and is proportional to the bandwidth of the pulse. By reducing the width of the slit between the two gratings, and thereby reducing the bandwidth, we decreased the stretch to ~20 ps, close to the resolution limit of the streak camera.

In the three-grating configuration the ray-tracing simulation gave a slope of $\approx 1800\ \mathrm{fs}^2$ at 800 nm, which led to a pulse stretch of 106 fs [Eq. (3)], in good agreement with the experimentally observed duration of 110 fs.

Our design can be used not only to separate a given harmonic without temporally stretching it but also to eliminate a (linear) chirp in the original pulse. We verified this by changing the distance between the compressor gratings of the Ti:sapphire laser system, thus stretching the pulse in time and imparting a linear chirp. By reoptimizing the angle of incidence on the transmission grating in our setup by a few degrees, we could compress the output pulse back to 110 fs.

4. Predictions and Discussion for the Extreme-Ultraviolet Range

We used the programs to optimize the setup for the XUV spectral range. Table 2 presents numerical results for stretches of the 9th, 17th, 33rd, and 65th harmonics of an 800-nm laser pulse in the two- and three-grating configurations for several groove densities of the spherical gratings. The divergence of the harmonics was assumed to be 2 mrad, and the bandwidth 100 THz, to simulate pulses generated with a 30-fs laser.[43] The radius of curvature of the spherical gratings was chosen to be 0.5 m, and the angle of incidence on the first grating was 40°. For each case the line density of the transmission grating was optimized by the ray-tracing program. The stretch depends strongly on the groove density of the spherical gratings as well as on the harmonic order. In the three-grating configuration there is also a more-complex dependence on the beam divergence. With three gratings, the main cause of the remaining temporal stretch is pulse-front distortion. For a 2-mrad-divergence high harmonic, even in the most difficult situation (i.e., for high groove density and a low-frequency harmonic) the pulses are stretched by only 3.9 fs. When spherical gratings with 400 lines/mm were chosen, the stretch is less than 1 fs for both the 9th- and 17th-harmonic orders. The stretch decreases rapidly with harmonic order.

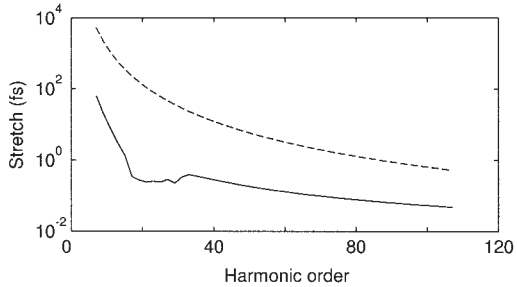

Fig. 9. Temporal stretch for the two-grating (dashed curve) and the three-grating (solid curve) setups. The line density is 800 lines/mm for the spherical gratings and 1000 lines/mm for the transmission grating.

For sufficiently high orders (depending on the characteristics of the spherical grating), the two-grating configuration can be used efficiently for selecting the harmonic radiation without temporal stretching.[23] The amount of residual stretch calculated for the 17th harmonic in the two-grating case is consistent with the experimental measurements of Nugent-Nandorf and co-workers,[24] suggesting a residual stretch in their toroidal–spherical grating configuration of at least 100 fs.

In Fig. 9 we show how the stretch for a given two- or three-grating configuration varies as a function of harmonic order. The spherical grating's line density was 800 lines/mm. The transmission grating's line density was chosen to be 1000 lines/mm, which optimizes the spectral region from the 17th to the 33rd order. The angle of the transmission grating was adjusted to yield the minimum stretch. The stretch decreases rapidly with order in both cases. The three-grating setup clearly minimizes the temporal stretch compared with the two-grating setup, even in a spectral region where the line density is not optimized.

Finally, we calculated the variation of the GD as a function of wavelength in a spectral region corresponding to the 17th harmonic (centered at 47 nm) for the line densities used in Fig. 9. Some results are shown in Fig. 10. As in Fig. 6, the chief and marginal rays that simulate beam divergence are represented. In Fig. 10(b), the angle of the transmission

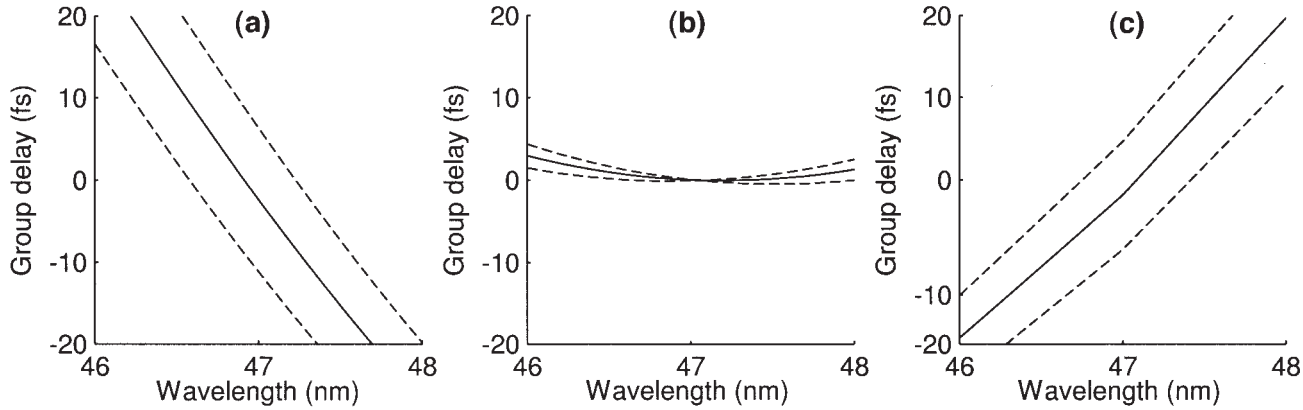

Fig. 10. GD for the chief and marginal rays as a function of wavelength for the 17th harmonic. In (b) the angle of the transmission grating (1000 lines/mm) has been adjusted to produce the minimum stretch. In (a) and (c) it was adjusted to compensate for (a) positive or (c) negative chirp of the XUV pulse.

grating was chosen such as to minimize the stretch. In Figs. 10(a) and 10(c), respectively, we chose the angle of the grating to compensate for a positive and a negative linear chirp rate of $\sim 2.5 \times 10^{28}$ fs^2, which is higher than the chirp rates measured experimentally so far.[44] This technique should allow us to compensate for rather important chirps that are due to the fundamental laser field, to propagation effects in the nonlinear medium, and to the generation process itself.

The simulation programs use a simplified two-dimensional model that includes spherical aberrations but does not take into account the astigmatism caused by the large incidence angle on the gratings. However, astigmatism can be eliminated by the use of toroidal gratings. The overall throughput of the proposed monochromator is also an important parameter to consider. Transmission gratings in the XUV range can have a relatively high throughput[45] and nowadays can be manufactured over a dimension of a few millimeters squared, thus matching the size required for the proposed setup. Using blazed gratings optimized for a certain wavelength region (e.g., 20–30 eV), we estimated the total transmission to be approximately 0.1%. With typical harmonic generation efficiencies of 10^{-6}–10^{-7} and laser pulse energies of a few millijoules this gives a photon flux of as much as 10^6–10^7 photons/pulse in a given harmonic order after spectral separation, which is enough for many applications.

We acknowledge the support of the Swedish Research Council, the European Community's programs "Training and Mobility of Researchers" (contract ERBFMGECT 980095, FIRE) and "Improving the Human Potential" (contracts HPRN-CT-2000-00133, ATTO, and HPRI-CT-2001-50037, SHARP), the Hungarian Academy of Sciences (contract OTKA T33018), and the Göran Gustafsson Foundation for Research in Natural Sciences and Medicine. D. Descamps acknowledges the support of the European Community's program "Training and Mobility of Researchers" (ERBFMBICT 983348, Marie Curie). Finally, we thank P. Villoresi for stimulating discussions.

References

1. J. J. Macklin, J. D. Kmetec, and C. L. Gordon III, "High-order harmonic generation using intense femtosecond pulses," Phys. Rev. Lett. **70,** 766–769 (1993).
2. A. L'Huillier and Ph. Balcou, "High-order harmonic generation in rare gases with a 1-ps 1053-nm laser," Phys. Rev. Lett. **70,** 774–777 (1993).
3. J. Larsson, E. Mevel, R. Zerne, A. L'Huillier, C.-G. Wahlström, and S. Svanberg, "Two-colour time-resolved spectroscopy of helium using high-order harmonics," J. Phys. B **28,** L47–L52 (1995).
4. P. Cacciani, W. Ubachs, P. C. Hinnen, C. Lyngå, A. L'Huillier, and C.-G. Wahlström, "Lifetime measurements of the $E\,^1\Pi$, $v = 0$ and $v = 1$ states of $^{12}C^{16}O$, $^{13}C^{16}O$, and $^{13}C^{18}O$," Astrophys. J. **499,** L223–L226 (1998).
5. R. Haight and D. R. Peale, "Antibonding state on the Ge(111):As surface: spectroscopy and dynamics," Phys. Rev. Lett. **70,** 3979–3982 (1993).
6. L. Nugent-Glandorf, M. Scheer, D. A. Samuels, A. M. Mulhisen, E. R. Grant, X. Yang, V. M. Bierbaum, and S. R. Leone, "Ultrafast time-resolved soft x-ray photoelectron spectroscopy of dissociating Br-2," Phys. Rev. Lett. **87,** 193002 (2001).
7. T. Sekikawa, T. Ohno, T. Yamazaki, Y. Nabekawa, and S. Watanabe, "Pulse compression of a high-order harmonic by compensating the atomic dipole phase," Phys. Rev. Lett. **83,** 2564–2567 (1999).
8. D. Descamps, L. Roos, C. Delfin, A. L'Huillier, and C.-G. Wahlström, "Two- and three-photon ionization of rare gases using femtosecond harmonic pulses generated in a gas medium," Phys. Rev. A **64,** 031404 (2001).
9. D. Descamps, C. Lyngå, J. Norin, A. L'Huillier, C.-G. Wahlström, J.-F. Hergott, H. Merdji, P. Salières, M. Bellini, and T. W. Hänsch, "Extreme ultraviolet interferometry measurements with high-order harmonics," Opt. Lett. **25,** 135–137 (2000).
10. A. Rundquist, C. G. Durfee III, Z. Chang, C. Herne, S. Backus, M. M. Murnane, and H. C. Kapteyn, "Phase-matched generation of coherent soft x-rays," Science **280,** 1412–1415 (1998).
11. Y. Tamaki, Y. Nagata, M. Obara, and K. Midorikawa, "Phase-matched high-order-harmonic generation in a gas-filled hollow fiber," Phys. Rev. A **59,** 4041–4044 (1999).
12. C. Lyngå, A. L'Huillier, and C.-G. Wahlström, "High order

harmonic generation in molecular gases," J. Phys. B **29,** 3293–3302 (1996).
13. P. Salières, A. L'Huillier, and M. Lewenstein, "Coherence control of high-order harmonics," Phys. Rev. Lett. **74,** 3776–3779 (1995).
14. Z. Chang, A. Rundquist, H. Wang, M. M. Murnane, and H. C. Kapteyn, "Generation of coherent soft x-rays at 2.7 nm using high harmonics," Phys. Rev. Lett. **79,** 2967–2970 (1997).
15. M. Schnürer, Ch. Spielmann, P. Wobrauschek, C. Streli, N. H. Burnett, C. Kan, K. Ferencz, R. Koppitsch, Z. Cheng, T. Brabec, and F. Krausz, "Coherent 0.5-keV x-ray emission from helium driven by a sub-10-fs laser," Phys. Rev. Lett. **80,** 3236–3239 (1998).
16. A. N. Zaidel and E. Y. Shreider, *Vacuum Ultraviolet Spectroscopy* (Ann Arbor–Humphrey Science, London, 1970), pp. 53–59.
17. O. E. Martinez, "3000 times grating compressor with positive group velocity dispersion," IEEE J. Quantum Electron. **QE-23,** 59–64 (1987).
18. A. M. Weiner, "Femtosecond pulse shaping and processing," Prog. Quantum Electron. **19,** 161–237 (1995).
19. I. Walmsley, L. Waxer, and C. Dorrer, "The role of dispersion in ultrafast optics," Rev. Sci. Instrum. **72,** 1–29 (2001).
20. G. Cheriaux, P. Rousseau, F. Salin, J. P. Chambaret, B. Walker, and L. F. Dimauro, "Aberration-free stretcher design for ultrashort-pulse amplification," Opt. Lett. **21,** 414–416 (1996).
21. J. Itiani, Y. Nabekawa, K. Kondo, and S. Watanabe, "Generation of 13TW, 26fs pulses in a Ti:sapphire laser," Opt. Commun. **134,** 134–138 (1997).
22. E. Goulielmakis, G. Nersisyan, N. A. Papadogiannis, D. Charalambidis, G. D. Tsakiris, and K. Witte, "A dispersionless Michelson interferometer for the characterization of attosecond pulses," Appl. Phys. B **74,** 197–206 (2002).
23. P. Villoresi, "Compensation of optical path lengths in extreme-ultraviolet and soft-x-ray monochromators," Appl. Opt. **38,** 6040–6049 (1999).
24. L. Nugent-Glandorf, M. Scheer, D. A. Samuels, V. Bierbaum, and S. R. Leone, "A laser-based instrument for the study of ultrafast chemical dynamics by soft x-ray probe photoelectron spectroscopy," Rev. Sci. Instrum. **73,** 1875–1886 (2002).
25. J.-C. Diels and W. Rudolph, *Ultrashort Laser Pulse Phenomena* (Elsevier, London, 1996), Chap. 2.6.
26. A. E. Siegman, *Lasers* (University Science, Mill Valley, Calif., 1986), Chap. 9.3.
27. W. Rudolph and B. Wilhelmi, *Light Pulse Compression* (Harwood Academic, Chur, Switzerland, 1989).
28. P. Lazaridis, G. Debarge, and P. Gallion, "Time–bandwidth product of chirped sech^2 pulses: application to phase–amplitude-coupling factor measurement," Opt. Lett. **20,** 1160–1162 (1995).
29. Z. Bor and B. Racz, "Group velocity dispersion in prisms and its application to pulse compression and travelling wave excitation," Opt. Commun. **54,** 165–170 (1985).
30. O. E. Martinez, "Pulse distortions in tilted pulse schemes for ultrashort pulses," Opt. Commun. **59,** 229–232 (1986).
31. O. E. Martinez, "Grating and prism compressors in the case of finite beam size," J. Opt. Soc. Am. B **3,** 929–934 (1986).
32. G. Pretzler, A. Kasper, and K. J. Witte, "Angular chirp and tilted light pulses in CPA lasers," Appl. Phys. B **70,** 1–9 (2000).
33. J. Hebling, "Derivation of the pulse front tilt caused by angular dispersion," Opt. Quantum Electron. **28,** 1759–1763 (1996).
34. Z. L. Horváth, K. Osvay, and Z. Bor, "Dispersed femtosecond pulses in the vicinity of the focus," Opt. Commun. **111,** 478–482 (1994).
35. R. A. Sawyer, *Experimental Spectroscopy* (Dover, New York, 1963).
36. C. M. Gonzalez Inchauspe and O. E. Martinez, "Aberration compensation of a curved diffraction grating stretcher for femtosecond chirped-pulse amplification," J. Opt. Soc. Am. B **14,** 2696–2700 (1997).
37. Z. Bor, "Distortion of femtosecond laser pulses in lenses," Opt. Lett. **14,** 119–121 (1989).
38. Z. Bor and Z. L. Horvath, "Distortions of femtosecond pulses in lenses: wave optical description," Opt. Commun. **94,** 249–258 (1992).
39. M. Kempe and W. Rudolph, "Impact of chromatic and spherical aberration on the focusing of ultrashort light pulses by lenses," Opt. Lett. **18,** 137–139 (1993).
40. E. B. Treacy, "Optical pulse compression with diffraction gratings," IEEE J. Quantum Electron. **QE-5,** 454–458 (1969).
41. S. D. Brorson and H. A. Haus, "Diffraction gratings and geometrical optics," J. Opt. Soc. Am. B **5,** 247–248 (1988).
42. G. O. Mattei and M. A. Gil, "Spherical aberration in spatial and temporal transforming lenses of femtosecond laser pulses," Appl. Opt. **38,** 1058–1064 (1999).
43. P. Villoresi, P. Ceccherini, L. Poletto, G. Tondello, C. Altucci, R. Bruzzese, C. de Lisio, M. Nisoli, S. Stagira, G. Cerullo, S. De Silvestri, and O. Svelto, "Spectral features and modeling of high-order harmonics generated by sub-10-fs pulses," Phys. Rev. Lett. **85,** 2494–2497 (2000).
44. R. López-Martens, J. Mauritsson, P. Johnsson, K. Varjú, A. L'Huillier, W. Kornelis, J. Biegert, U. Keller, M. B. Gaarde, and K. J. Schafer, "Towards the tailoring of high-order harmonic emission," Appl. Phys. B (to be published).
45. K. Eidmann, M. Kühne, P. Müller, and G. D. Tsakiris, "Characterization of pinhole transmission gratings," J. X-Ray Sci. Technol. **2,** 259–273 (1990).